

Direct Aromatic ^{18}F -Labeling of Highly Reactive Tetrazines for Pretargeted Bioorthogonal PET Imaging

Rocío García-Vázquez^{a,*}, Umberto M. Battisti^{a,*}, Jesper T. Jørgensen^{b,c}, Vladimir Shalgunov^{a,b}, Lars Hvass^{b,c}, Daniel L. Stares^a, Ida N. Petersen^b, François Crestey^a, Andreas Löffler^d, Dennis Svatunek^d, Jesper L. Kristensen^a, Hannes Mikula^d, Andreas Kjaer^{b,c,#}, Matthias M. Herth^{a,c,#}

^aDepartment of Drug Design and Pharmacology, Faculty of Health and Medical Sciences, University of Copenhagen, Jagtvej 160, 2100 Copenhagen, Denmark; ^bCluster for Molecular Imaging, Department of Biomedical Sciences, University of Copenhagen, Blegdamsvej 9, 2100 Copenhagen, Denmark; ^cDepartment of Clinical Physiology, Nuclear Medicine & PET, Rigshospitalet, Blegdamsvej 9, 2100 Copenhagen, Denmark; ^dInstitute of Applied Synthetic Chemistry, Technische Universität Wien (TU Wien), Getreidemarkt 9, 1060 Vienna, Austria. * These authors contributed equally to this work. #Corresponding authors

Abstract: Pretargeted bioorthogonal imaging can be used to visualize and quantify slow accumulating targeting vectors with short-lived radionuclides such as fluorine-18 - the most clinically applied Positron Emission Tomography (PET) radionuclide. Pretargeting results in higher target-to-background ratios compared to conventional imaging approaches using long-lived radionuclides. Currently, the tetrazine ligation is the most popular bioorthogonal reaction for pretargeted imaging, but a direct ^{18}F -labeling strategy for highly reactive tetrazines, which would be highly beneficial if not essential for clinical translation, has thus far not been reported. In this work, a simple, scalable and reliable direct ^{18}F -labeling procedure has been developed and applied to obtain a pretargeting tetrazine-based imaging agent with favorable characteristics (target-to-background ratios and clearance) that may qualify it for future clinical translation.

Positron-Emission-Tomography (PET) is a powerful, non-invasive and routinely used imaging tool in precision medicine or drug development.^[1-3] Its high sensitivity (the level of detection approaches 10^{-12} M of tracer), isotropism and quantitativity are in combination unmatched compared to any other *in vivo* molecular imaging technique.^[4, 5] Fluorine-18 (^{18}F) is considered as the best suited PET radionuclide for clinical applications as it provides almost ideal physical characteristics for molecular imaging. These include a relatively short positron range (2.4 mm max. range in water), a good branching ratio (96.7% positron decay) and a half-life of approx. 110 min, that enables to distribute ^{18}F -labeled tracers within a several hundred kilometers range.^[6-8] Recently, bioorthogonal chemistry has emerged as a versatile tool for pretargeted nuclear imaging of slow-accumulating targeting vectors such as monoclonal antibodies (mAbs) or other nanomedicines.^[9-11] Improved imaging contrast (up to 100-fold) and lower radiation burden to healthy tissue can be achieved using pretargeting compared to conventional imaging strategies.^[10] These improved imaging characteristics are a result of the temporal separation of the slow targeting process of nanomedicines from the actual imaging step. Consequently, the exceptional target specificity of nanomedicines as well as the optimal pharmacokinetics of small molecules for molecular imaging, e.g. selective target accumulation and rapid clearance from blood, can be exploited using pretargeted imaging.^[12, 13] So far, the most prominent reaction for pretargeted imaging is the tetrazine (Tz) ligation. Excellent chemoselectivity, metabolic stability and high reactivity make the Tz ligation as exceptional as the biotin-(strept)avidin interaction for pretargeting strategies.^[14-17] The Tz ligation is driven by the Inverse-Electron-Demand Diels-Alder (IEDDA) cycloaddition between an electron-deficient Tz and strained trans-cyclooctene (TCO) derivative, followed by a retro-Diels-Alder elimination of nitrogen.^[10, 18-20] Despite efforts focused on TCO-based click imaging agents^[21, 22], the use of radiolabeled Tz has gradually emerged in recent literature.^[10]

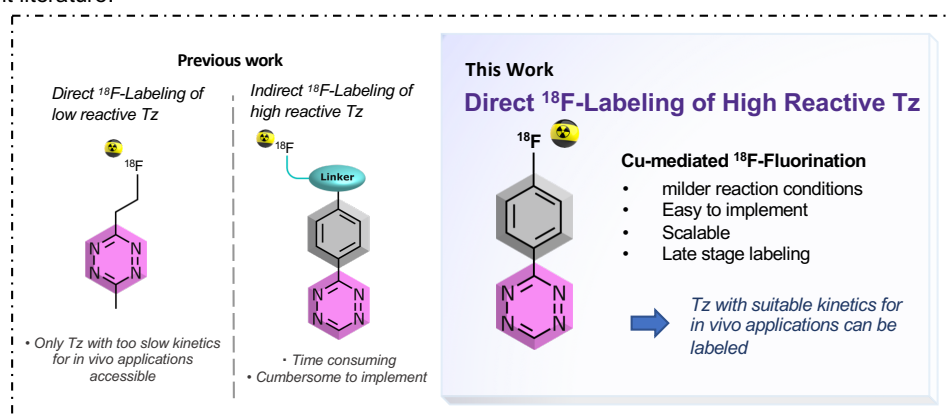


Figure 1. Comparison of previously reported ^{18}F -labeling strategies of tetrazines vs the direct aromatic ^{18}F -labeling approach developed in this work.

Throughout the last decade, the labeling of Tzs was mostly limited to chelation of radiometals such as ^{64}Cu , ^{89}Zr , ^{44}Sc or ^{68}Ga .^[23-27] In 2013, the first successful attempt to label a Tz moiety with a covalently bound PET radionuclide, i.e. with carbon-11, was reported by our group.^[28] Despite significant progress in the field, until recently all reported ^{18}F -Tzs had electron-donating alkyl substituents at the Tz ring and thus had low reactivity towards TCOs.^[17] The reason for this is that highly reactive mono- or bis-(hetero)aryl-substituted Tzs decompose under the harsh conditions used for standard nucleophilic ^{18}F -fluorination ($\text{S}_{\text{N}}2$ or $\text{S}_{\text{N}}\text{Ar}$) approaches.^[11, 17, 29] Only relatively base insensitive and less reactive Tzs could be radiolabeled, via an ^{18}F -aliphatic substitution ($\text{S}_{\text{N}}2$) strategy. Radiochemical yields (RCYs) up to 18% were achieved.^[17] More recently, the preparation of a highly reactive ^{18}F -labeled glycosylated Tz by Keinänen and co-workers and an [^{18}F]AIF-NOTA-labeled Tz radioligand by Meyer and co-workers were reported.^[27, 29] For the latest strategy added to this portfolio, we exploited the copper-catalyzed azide-alkyne cycloaddition to

efficiently label highly reactive Tzs.^[11, 17] However, none of the aforementioned ¹⁸F-labeling procedures seem optimal for clinical applications. Multi-step procedures are usually challenging to set up for clinical routine, while Al¹⁸F-labeling procedures are challenging to scale up.^[30-32] For these reasons, we aimed to develop a simple, scalable and reliable direct aromatic radiofluorination procedure that can be applied to access highly reactive ¹⁸F-labeled Tzs (Figure 1). Ultimately, such procedure would pave the way to develop a ¹⁸F-Tz based pretargeted imaging agent with favorable reaction kinetics, good metabolic stability and the pharmacokinetic profile required for bioorthogonal *in vivo* chemistry.

The synthesis of most ¹⁸F-fluorinated aryls is based on nucleophilic aromatic substitution (S_NAr) strategies.^[8, 33-35] Typically, this type of reactions requires relatively strong basic conditions and high temperature, and as such, the S_NAr is not ideally suited to ¹⁸F-label structures containing highly reactive Tz moieties which are known to be base-sensitive.^[17, 36] Recently, several milder aromatic ¹⁸F-labeling strategies have been reported that proceed at lower temperatures and in short reaction times, while using less basic reaction conditions. Especially, Cu-mediated oxidative fluorinations of tin and boronic esters or acids^[37-41], concerted nucleophilic aromatic substitution of uronium or iodonium salts^[34, 42-44], hypervalent iodonium based precursors^[45-47] and minimalistic labeling strategies^[33, 35] have proven their potential in this respect. We decided to investigate all these strategies and explore if they could be utilized to synthesize ¹⁸F-labeled Tzs, with emphasis on highly reactive structures. Tz **6** was selected as a simple model as it is readily accessible and displays moderate stability against strong bases. This allows us to first study the suitability of these type of reactions before attempting the most promising strategy with base-sensitive Tz-scaffolds. Precursors **1-5** and reference compound **6** were synthesized similar to reported procedures (SI, Section S2).^[48, 49] In our hands, ¹⁸F-labeling strategies including minimalist approaches resulted in decomposition of the product. On the contrary, the Cu-mediated ¹⁸F-fluorination starting from a stannane precursor resulted in a radiochemical conversion (RCC) of approximately 14% at the first attempt (Figure 2A).⁵⁰ Further optimization of temperature, reaction time and amount of base led to an improvement to approx. 30% RCC (Figure 2B).

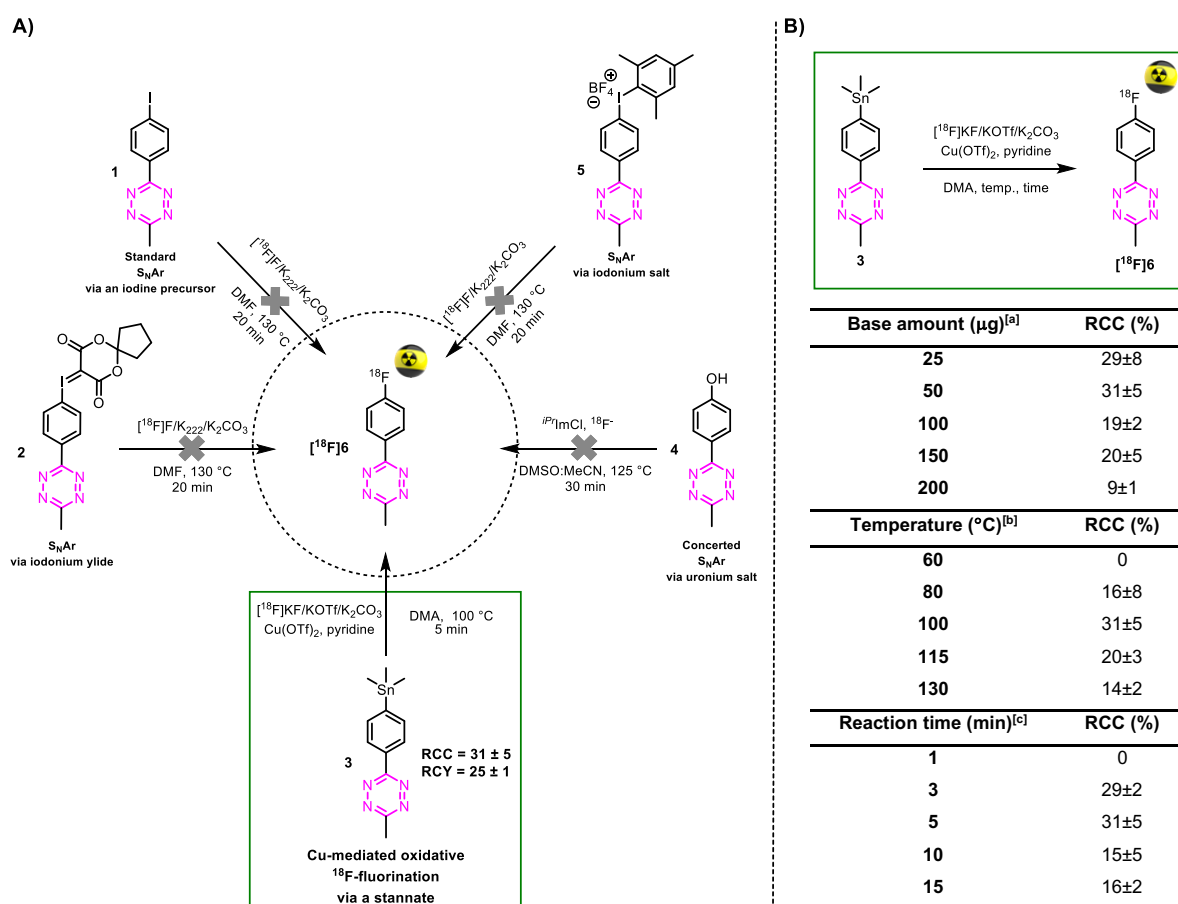
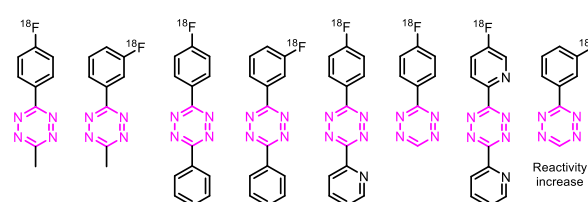


Figure 2. Proof of principle of ¹⁸F-labeling of a methyl-phenyl-Tz. **(A)** Radiolabeling strategies using different methyl-phenyl-Tz precursors. **(B)** Optimization of the Cu-mediated ¹⁸F-fluorination from stannane precursor **3** to [¹⁸F]**6**. [a] Conditions: Cu(OTf)₂, pyridine, [¹⁸F]KF, DMA, 100 °C, 5 min. [b] Conditions: Cu(OTf)₂, pyridine, [¹⁸F]KF (50 μg K₂CO₃), DMA, 100 °C, 5 min. [c] Conditions: Cu(OTf)₂, pyridine, [¹⁸F]KF (50 μg K₂CO₃), DMA, 100 °C. Radiochemical conversion (RCC) was determined by radio-TLC and radio-HPLC (n=3). Radiochemical yield (RCY) was decay corrected to the starting amount of radioactivity received from the cyclotron and the isolated product without formulation step (n=3).

With these encouraging results, we decided to study if more reactive Tzs could also be labeled using this strategy. Tzs with stepwise increased reactivity were selected to investigate the scope of our radiofluorination method (Table 1). Precursors and reference compounds were synthesized using known procedures (SI, Section S2)^[48, 51-53] and radiolabeling was conducted using the best conditions identified labeling our model compound. Moderate RCCs (12–31%) as well as sufficient decay-corrected (d.c.) RCYs (10–24%) were observed at the end of synthesis (EOS) for methyl-, phenyl- and H-Tzs (Table 1). The automated synthesis including [¹⁸F]fluoride concentration and drying, labeling, high-performance liquid chromatography (HPLC) separation and

formulation was carried out within 90 minutes (SI, Section S3). Radiochemical purity (RCP) was >99% for all prepared ^{18}F -fluorinated tetrazines, and a molar activity (A_m) was $190 \pm 10 \text{ GBq}/\mu\text{mol}$ (d.c) ($n=3$) for $[^{18}\text{F}]\mathbf{6}$, which is in line with the results obtained for other tracers on the used module and the same starting activity. A typical activity yield was 2.5–3 GBq starting from ~12 GBq fluoride-18. Pyridyl structures could not be labeled using this labeling strategy, most likely due to a chelation of the copper ion with the respective pyridyl moieties of the Tz.^[54] As expected, the most reactive Tz resulted in the lowest RCY. However, the observed RCYs are in the range of many clinically applied PET tracers.^[38, 39, 55]

Table 1. Product scope for the Cu-mediated ^{18}F -fluorination of aryl-tetrazines.



Compound	$[^{18}\text{F}]\mathbf{6}$	$[^{18}\text{F}]\mathbf{7}$	$[^{18}\text{F}]\mathbf{8}$	$[^{18}\text{F}]\mathbf{9}$	$[^{18}\text{F}]\mathbf{10}$	$[^{18}\text{F}]\mathbf{11}$	$[^{18}\text{F}]\mathbf{12}$	$[^{18}\text{F}]\mathbf{13}$
RCC ^[a] [%]	30±5	28±1	30±5	31±2	↓ ^[d]	18±4	↓ ^[d]	12±1
RCY ^[b] [%]	23±1	26±2	23±2	24±3	↓ ^[d]	15±3	↓ ^[d]	11±3
Rel. reactivity ^[c]	1.0	1.4	1.8	3.0	10	70	91	96
RCP ^[a] [%]	≥99	≥99	≥99	≥99	↓ ^[d]	99	↓ ^[d]	99

[a] Radiochemical conversion (RCC) and radiochemical purity (RCP) were determined by radio-HPLC and radio-TLC ($n=3$).
 [b] Radiochemical yield (RCY) was decay corrected to the starting amount of radioactivity received from the cyclotron and the isolated product without a formulation step ($n=3$).
 [c] Relative IEDDA reactivity was calculated based on second order rate constants determined by stopped-flow measurements of the respective reference compound (^{18}F -Tz) with *trans*-cyclooctene at 25 °C in 1,4-dioxane or acetonitrile (see Supporting Information).
 [d] No product could be isolated.

Table 2. Product scope in respect to different substituted phenyl-Tz for the Cu-mediated ^{18}F -fluorination.



R	Compound	Position		
	(-p, -m, -o)	4 (-p)	5 (-m)	6 (-o)
-CH ₃	$[^{18}\text{F}]\mathbf{14}$	↓ ^[a]	14±3 ^[b]	↓ ^[c]
-OCH ₃	$[^{18}\text{F}]\mathbf{15}$	4±1	17±3 ^[b]	↓ ^[c]
-NHCOCH ₃	$[^{18}\text{F}]\mathbf{16}$	↓ ^[a]	31±3 ^[b]	↓ ^[d]
-CONH ₂	$[^{18}\text{F}]\mathbf{17}$	↓ ^[a]	24±2 ^[b]	↓ ^[d]
-CONHCH ₃	$[^{18}\text{F}]\mathbf{18}$	↓ ^[a]	20±3 ^[b]	↓ ^[d]

[a] Stannane precursor could not be synthesized.
 [b] RCCs were determined by radio-HPLC and radio-TLC ($n=3$).
 [c] Decomposed during the Cu-mediated ^{18}F -fluorination.
 [d] Iodo-Tz intermediate could not be synthesized.

To study the effect of different substituents at the aryl ring, $[^{18}\text{F}]\mathbf{13}$ was selected for further analysis since it displayed the highest relative IEDDA reactivity. The IEDDA reactivity is one of the most crucial factors for pretargeted *in vivo* applications.^[11] Electron-donating and electron-withdrawing substituents were introduced on the phenyl moiety at different positions, and the substitution pattern was correlated with its synthetic accessibility and RCCs (used as a surrogate for RCYs, RCC correlated with RCY in our study) (Table 2). While all 5-substituted stannane precursors were successfully synthesized from respective iodo-Tz intermediates, only the methyl and/or methoxy derivatives among 4- and 6-substituted stannanes could be prepared - most likely due to steric hindrance.^[37-39] During ^{18}F -fluorinations, only 3,5-disubstituted stannane precursors provided useful RCCs in the order of 14–31%. No or only minimal product formation could be observed with a different substitution profile (Table 2). Hence, the 3,5-disubstitution pattern was identified to be best suited for Cu-mediated oxidative ^{18}F -fluorinations. Recently, our group has demonstrated that the performance of Tz-derivatives and probes for pretargeted *in vivo* ligation strongly depends on the lipophilicity and the IEDDA reactivity of the Tz agent. Low polarity ($\text{clogD}_{7.4} < -3$) and rate constants $>50,000 \text{ M}^{-1}\text{s}^{-1}$ for the click reaction with axially configured TCO tags (Dulbecco's PBS, 37 °C) resulted in best target-to-background ratios.^[11] In this respect, we designed two highly reactive Tzs, which contained polar groups and allowed for direct ^{18}F -labeling. Tz **19** possesses a $\text{clogD}_{7.4}$ of -3.09 and a rate constant of $91,000 \text{ M}^{-1}\text{s}^{-1}$, and Tz **21** a $\text{clogD}_{7.4}$ of -6.93 and a rate constant of $82,000 \text{ M}^{-1}\text{s}^{-1}$ (SI, Section S5). Both compounds were synthesized in sufficient yields via a Pinner-like synthesis (SI, Section S2) and evaluated in an *in vivo* assay recently described by our group (Figure 3A).^[11] This assay, inspired by traditional receptor blocking studies, applies anti-TAG72 mAb CC49 modified with axially configured TCO tags (CC49-TCO) and [^{111}In]DOTA-Tz (**22**), which has previously successfully been used for pretargeted imaging in (TAG72 expressing) LS174T tumors.^[24] In short, tumor-bearing mice are injected with a CC49-TCO, 72 h before the non-labeled Tz to be tested. Subsequently, [^{111}In]DOTA-Tz (**22**) is injected after 1 h and a biodistribution is performed 22 h later (SI, Section S5).^[11, 24] The assay evaluates the blocking ability of the non-labeled Tz, and allows therefore estimation of the *in vivo* ligation performance of this compound. Higher blocking capacity is correlated with better *in vivo* performance of the respective Tz.^[11] As expected - based on our previous data - we found a correlation between $\text{cLogD}_{7.4}$ and *in vivo* blocking of the Tzs tested in the assay (Pearson's $r = 0.89$, $p < 0.01$) and the most polar Tz **21** ($\text{clogD}_{7.4} = -6.93$) resulted in the best blocking effect (90%) (Figure 3B) was selected for further development.

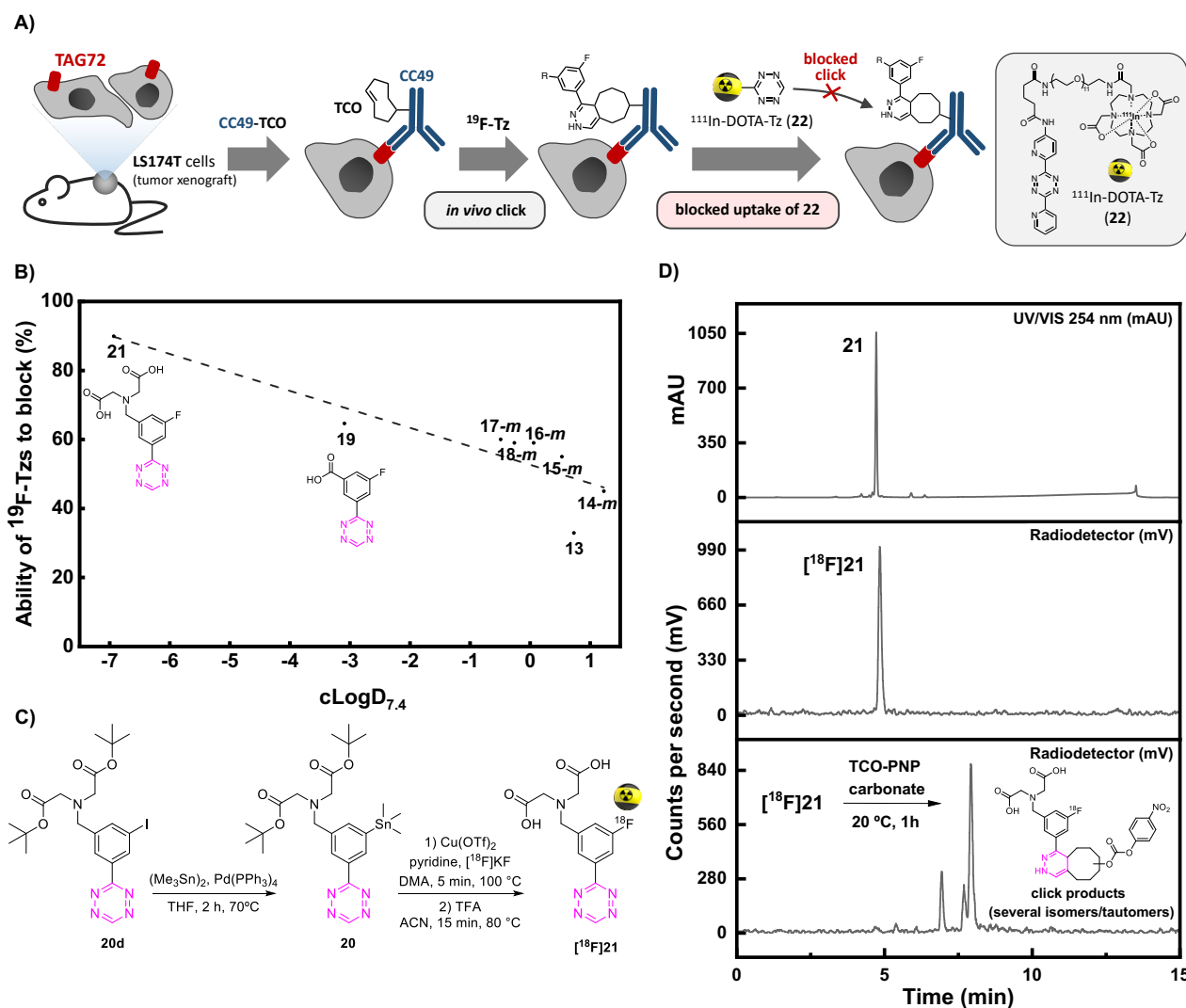


Figure 3. (A) Visualization of the blocking assay (B) Ability of ^{19}F -Tzs (**13**, **14-m**–**18-m**, **19**, **21**) to block ^{111}In -DOTA-Tz (**22**) in an *in vivo* screening assay for pretargeted ligation ($n=3$) (SI, Section S5). (C) Synthesis and radiolabeling of ^{18}F 21. (D) Analytical-HPLC of reference compound **21** (UV/Vis, 254 nm) (Upper panel), radio-HPLC of purified ^{18}F 21 (middle panel) and ligation product after click reaction with the TCO-PNP carbonate (**23**), one-hour post-injection (lower panel). Analytical HPLC conditions: Luna 5 μm C18(2) 100 Å, 150 mm \times 4.6 mm; Eluents: A, H_2O with 0.1% TFA; B, MeCN with 0.1% TFA; Gradient from 100% A to 100% B over 12 min, back to 100% A over 3 min, flow rate 2 mL/min.

The shelf stability of Tz **21** was assessed in phosphate-buffered saline (PBS) by analytical-HPLC. Compound **21** did not show degradation in PBS after 12 h at 37 °C at a concentration of 2 nmol/mL (98%). Consequently, the stannane precursor was synthesized in 4 steps (SI, Section S2). Radiolabeling succeeded in a one-pot, two-step sequence with a RCY (d.c.) of 11 \pm 3% ($n = 4$) and an overall synthesis time of ca. 90 minutes including synthesis, separation and formulation. ^{18}F 21 was obtained with an A_m of 134 \pm 22 GBq/ μmol (d.c.), a RCP of \geq 99% ($n=4$) and an activity yield of 600–700 MBq (EOS) starting from \sim 12 GBq fluoride-18 (Figure 3C and D). ^{18}F 21 was stable in PBS at room temperature for minimum 4 h and rapidly reacted with TCO-PNP carbonate (**23**) as confirmed by radio-HPLC (Figure 3D and SI, Section S3). Residual amounts of Cu and Sn in the final formulated solution were analyzed by ICP-MS and found to be well below the allowed limits specified in the ICH Guidelines (41–60 and 2.3–3.0 $\mu\text{g/L}$ vs. 300 and 600 $\mu\text{g/day}$, respectively).^[38, 56-58]

Next, we evaluated the performance of ^{18}F 21 in pretargeted PET imaging (Figure 4A). Balb/c nude mice bearing LS174T tumor xenografts ($n = 3$ per group) were injected i.v. with either CC49-TCO (100 μg , 3.9 nmol, \sim 7 TCO/mAb) or non-modified CC49 (control). After 72 h, ^{18}F 21 (2.86 \pm 0.99 MBq/100 μL) was administered and the mice were PET/CT scanned after 1 h. Image-derived uptake in tumor, heart (surrogate for blood) and muscle tissue was quantified as percentage injected dose per gram (mean % ID/g), (Figure 4B, C, D and E). After completion of the scan, mice were euthanized and *ex vivo* biodistribution was performed (SI, Section S6). Mice pretreated with CC49-TCO demonstrated a mean tumor uptake of ^{18}F 21 of 0.99 \pm 0.14 %ID/g (mean \pm S.E.M.). The tracer displayed good target-to-background ratios with muscle uptake < 0.15 %ID/g for all animals (Table S9). This was also evident from PET/CT images, where tumor uptake in the CC49-TCO group was clearly visible (Figure 4E). The mean tumor-to-blood ratio was 0.9, and thereby the specific uptake is similar to what was previously reported for other pretargeted imaging agents in the same tumor model.^[11] In contrast, a mean tumor-to-muscle ratio of 10 was detected which in fact is significantly higher compared to what has previously been found for the “state-of-the-art” Tz-based imaging agents ^{18}F 22 and ^{64}Cu [Cu-NOTA-PEG7-H-Tz - in a similar pretargeting set-up (LS174T bearing mice, using CC49-TCO 72h prior to tracer injection, similar imaging timeframes) (Figure 4C and D).^[25, 59] However, ^{18}F 21 showed a 3 to 5-fold lower tumor uptake compared to those

imaging agents (Figure 4E).^[25, 59] All tissues including tumors showed low ¹⁸F-uptake in control animals (CC49) (tumor uptake of 0.05 ± 0.04 %ID/g). The findings from the imaging experiment were confirmed by *ex vivo* biodistribution data (Table S10). Except for the tumor, the only tissue, where the tracer uptake was significant, was blood. This accumulation is likely caused by the *in vivo* ligation of [¹⁸F]21 to CC49-TCO still circulating in the bloodstream. An observation that has been reported before for other pretargeting pairs.^[10] If residual mAbs are removed from the blood pool by e.g. a clearing agent, subsequent injection of [¹⁸F]21 will likely result in an improved tumor-to-blood ratio.^[10]

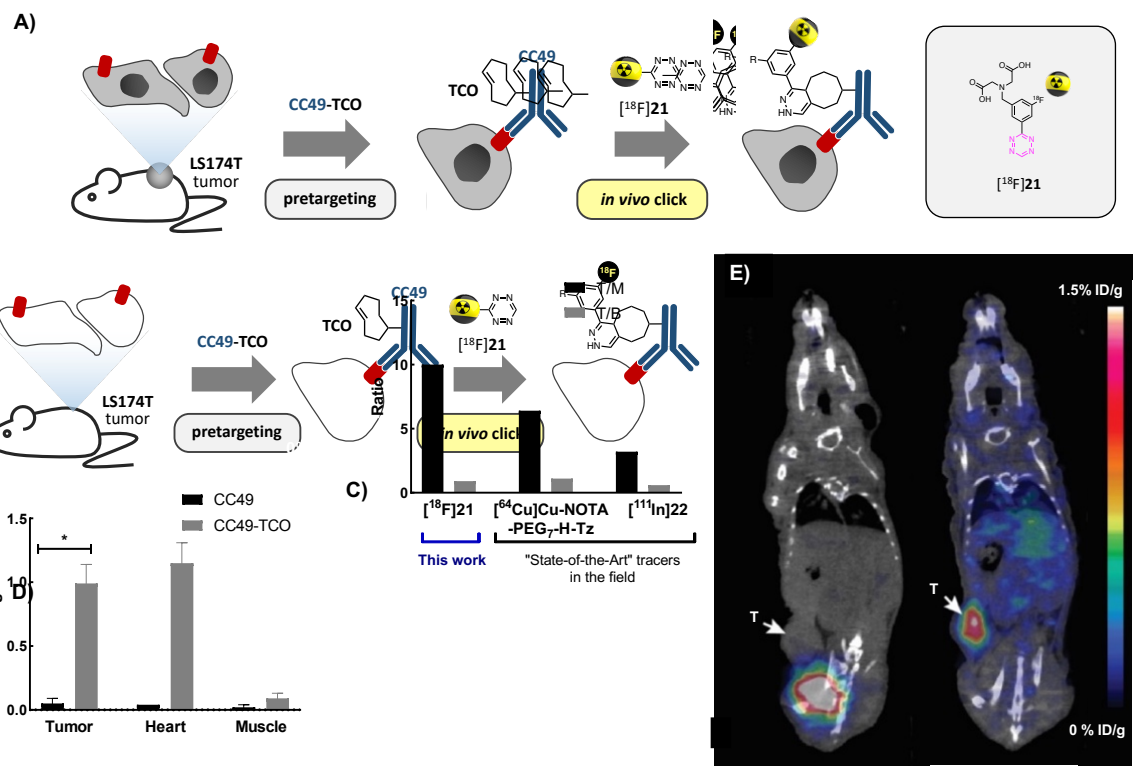


Figure 4: PET/CT scan of CC49-TCO pretargeted [¹⁸F]21 in LS174T tumor xenograft bearing mice. **(A)** General pretargeted imaging approach. **(B)** PET-Image derived mean %ID/g in tumor-, heart- and muscle tissue 1 h p.i. of [¹⁸F]21. mean ± S.E.M, n = 3/group. *p < 0.05 (Welch's t-test) **(C & D)** Image-derived tumor uptake (mean % ID/g), Tumor-to-muscle (T/M) and Tumor-to-Blood ratio (T/B) of [¹⁸F]21 in comparison with "state of the art" applied Tz imaging agents [⁶⁴Cu]Cu-NOTA-PEG₇-H-Tz (PET 2 h p.i., n = 4) and [¹¹¹In]22 (SPECT 2 h p.i., n = 4). Tumor uptake and ratios of [⁶⁴Cu]Cu-NOTA-PEG₇-H-Tz and [¹¹¹In]22 2 h p.i. in nude BALB/c mice bearing subcutaneous LS174T tumor xenografts pretreated with CC49-TCO (100 µg) has recently been published.^[25, 59] Data are shown as mean ± standard error of mean (SEM). *Image-derived uptake in heart from SPECT and PET images used as a surrogate for blood.^[25, 59] **(E)** Representative images from PET/CT-scans 1 h p.i. of [¹⁸F]21. Mice were administered with either non-modified CC49 (left) or CC49-TCO (right), 72 h prior to [¹⁸F]21 injection. Arrows indicate LS174T tumor xenografts. Scale bar indicates mean %ID/g.

In conclusion, this work enabled the first direct ¹⁸F-labeling of highly reactive Tzs starting from stannane precursors via a Cu-mediated approach. Applying this strategy, we have successfully prepared a new ¹⁸F-Tz, [¹⁸F]21, with highly favorable characteristics for pretargeted *in vivo* imaging. The developed procedure is simple, short, reproducible and scalable. Therefore, it is more suitable for clinical applications than previously used multistep ¹⁸F-labeling strategies. We are thus convinced that our method for the direct radiofluorination of highly reactive tetrazines will improve and accelerate the clinical translation of pretargeted imaging based *in vivo* click chemistries.

Acknowledgements

This project has received funding from the European Union's EU Framework Programme for Research and Innovation Horizon 2020, under grant agreement no. 668532. HM, AK and MMH have received funding from the European Union's EU Framework Programme for Research and Innovation Horizon 2020 (grant agreement no. 670261). VS was supported by BRIDGE – Translational Excellence Programme at the Faculty of Health and Medical Sciences, University of Copenhagen, funded by the Novo Nordisk Foundation (grant agreement no. NNF18SA0034956). The Lundbeck Foundation, the Novo Nordisk Foundation, the Innovation Fund Denmark, and the Research Council for Independent Research are further acknowledged. The modified antibody used in this study was kindly provided by Tagworks Pharmaceuticals.

Keywords: tetrazines • bioorthogonal chemistry • molecular imaging • cancer • pretargeted imaging • fluorine-18 • PET

References

- [1] J. L. Kristensen, M. M. Herth in *Textbook of Drug Design and Discovery*, 5th Edition (Eds. K. Strømgaard, P. Krosggaard-Larsen, U. Madsen), CRC Press, London and New York, **2017**, pp 119-136.
- [2] M. Piel, I. Vernaleken, *J. Med. Chem.* **2014**, *57*, 9232-9258.
- [3] B. Theek, L. Y. Rizzo, *Clin. Transl. Imaging* **2014** *2*, 67-76.
- [4] M. M. Herth, M. Barz, *Biomacromolecules* **2009** *10*, 1697-1703.
- [5] S. M. Ametamey, M. Honer, *Chem. Rev.* **2008** *108*, 1501-1516.
- [6] D. Le Bars, *J. Fluor. Chem.* **2006** *127*, 1488-1493.
- [7] X. Deng, J. Rong, *Angew. Chem. Int. Ed.* **2019** *58*, 2580-2605.
- [8] P. E. Edem, E. J. L. Stéen in *Late-Stage Fluorination of Bioactive Molecules and Biologically-Relevant Substrates*, 1st Edition (Eds. A. Postigo), Elsevier, Copenhagen, **2019**, pp. 29-103.
- [9] J. M. Baskin, J. A. Prescher, *Proc. Natl. Acad. Sci.* **2007** *104*, 16793-16797.
- [10] E. J. L. Stéen, P. E. Edem, *Biomaterials* **2018** *179*, 209-245.
- [11] E. J. L. Stéen, J. T. Jørgensen, **2020**, DOI 10.26434/chemrxiv.13482594.v1.
- [12] M. Patra, K. Zarschler, *Chem. Soc. Rev.* **2016** *45*, 6415-6431.
- [13] D. M. Goldenberg, R. M. Sharkey, *Journal of Clinical Oncology* **2006** *24*, 816.
- [14] N. K. Devaraj, R. Weissleder, *Acc. Chem. Res.* **2011** *44*, 816-827.
- [15] L. Carroll, H. L. Evans, *Org. Biomol. Chem.* **2013** *11*, 5772-5781.
- [16] M. T. Taylor, M. L. Blackman, *J. Am. Chem. Soc.* **2011** *133*, 9646-9649.
- [17] C. Denk, D. Svatunek, *Angew. Chem. Int. Ed.* **2014** *53*, 9655-9659.
- [18] B. L. Oliveira, Z. Guo, *Chem. Soc. Rev.* **2017** *46*, 4895-4950.
- [19] M. L. Blackman, M. Royzen, *J. Am. Chem. Soc.* **2008** *130*, 13518-13519.
- [20] E. J. L. Stéen, V. Shalgunov, *Eur. J. Org. Chem.* **2019** *2019*, 1722-1725.
- [21] D. Thomae, A. Waldron, *Nucl. Med. Biol.* **2014** *41*, 513-523.
- [22] E. M. F. Billaud, S. Belderbos, *Bioconjug. Chem.* **2017** *28*, 2915-2920.
- [23] M. R. Lewis, M. Wang, *J. Nucl. Med.* **2003** *44*, 1284-1292.
- [24] R. Rossin, P. Renart Verkerk, *Angew. Chem. Int. Ed.* **2010** *122*, 3447-3450.
- [25] P. E. Edem, J. T. Jørgensen, *Molecules* **2020** *25*, 463.
- [26] P. E. Edem, J. Sinnes, *EJNMMI research* **2019** *9*, 1-8.
- [27] J. Meyer, J. L. Houghton, *Bioconjug. Chem.* **2016** *27*, 298-301.
- [28] M. M. Herth, V. L. Andersen, *ChemComm* **2013** *49*, 3805-3807.

- [29] O. Keinänen, X. Li, *ACS Med. Chem. Lett.* **2015** *7*, 62-66.
- [30] D. Van Der Born, A. Pees, *Chem. Soc. Rev.* **2017** *46*, 4709-4773.
- [31] J. Zhu, S. Li, *ChemComm* **2015** *51*, 12415-12418.
- [32] O. Keinänen, X. Li, *ACS Med. Chem. Lett.* **2016** *7*, 62-66.
- [33] M. Tredwell, V. Gouverneur, *Angew. Chem. Int. Ed.* **2012** *51*, 11426-11437.
- [34] C. N. Neumann, J. M. Hooker, *Nature* **2016** *534*, 369-373.
- [35] S. Preshlock, M. Tredwell, *Chem. Rev.* **2016** *116*, 719-766.
- [36] Z. Li, H. Cai, *ChemComm* **2010** *46*, 8043-8045.
- [37] M. Tredwell, S. M. Preshlock, *Angew. Chem. Int. Ed.* **2014** *53*, 7751-7755.
- [38] K. J. Makaravage, A. F. Brooks, *Org. Lett.* **2016** *18*, 5440-5443.
- [39] S. Preshlock, S. Calderwood, *ChemComm* **2016** *52*, 8361-8364.
- [40] J. Zischler, N. Kolks, *Chem. Eur. J.* **2017** *23*, 3251-3256.
- [41] N. J. Taylor, E. Emer, *J. Am. Chem. Soc.* **2017** *139*, 8267-8276.
- [42] T. L. Ross, J. Ermert, *J. Am. Chem. Soc.* **2007** *129*, 8018-8025.
- [43] M. H. Beyzavi, D. Mandal, *ACS Cent. Sci.* **2017** *3*, 944-948.
- [44] Y. Kwon, J. Son, *J. Org. Chem.* **2019** *84*, 3678-3686.
- [45] I. N. Petersen, J. Villadsen, *Org. Biomol. Chem.* **2017** *15*, 4351-4358.
- [46] I. N. Petersen, J. L. Kristensen, *Eur. J. Org. Chem.* **2017** *2017*, 453-458.
- [47] I. Nyman Petersen, J. Madsen, *Molecules* **2019** *24*, 3436.
- [48] J. W. McIntee, C. Sundararajan, *J. Org. Chem.* **2008** *73*, 8236-8243.
- [49] J. Yang, M. R. Karver, *Angew. Chem. Int. Ed.* **2012** *51*, 5222-5225.
- [50] M.M. Herth, S. Ametamey, *Nuclear Medicine and Biology* **2021** *93*, 19-21.
- [51] Y. Qu, F. Sauvage, *Angew. Chem. Int. Ed.* **2018** *130*, 12233-12237.
- [52] J. Yang, M. R. Karver, *Angew. Chem. Int. Ed.* **2012** *51*, 5222-5225.
- [53] S. A. Albu, S. A. Al-Karmi, *Bioconjug. Chemistry* **2016** *27*, 207-216.
- [54] H. T. Chifotides, I. D. Giles, *J. Am. Chem. Soc.* **2013** *135*, 3039-3055.
- [55] J. Wang, W. Tueckmantel, *Synapse* **2007** *61*, 951-961.
- [56] Guideline for Elemental Impurities. In *Q3D; ICH: Geneva, Switzerland*, **2013**, pp.39-40.
- [57] M. S. Sanford, P. J. Scott, *ACS Cent. Sci.* **2016** *2*, 3, 128-130.
- [58] F. Zarrad, B. D. Zlatopolskiy, *Molecules* **2017** *22*, 2231.

[59] C. Poulie, J. T. Jørgensen, *Molecules* **2021** 26, 544.